Appl. Math. Mech. -Engl. Ed., **40**(12), 1777–1790 (2019)

Applied Mathematics and Mechanics (English Edition)

https://doi.org/10.1007/s10483-019-2542-5

Low-frequency and broadband vibration energy harvester driven by mechanical impact based on layer-separated piezoelectric beam*

Dongxing CAO[1,2,†], Wei XIA[1,2], Wenhua HU[3]

1. College of Mechanical Engineering, Beijing University of Technology, Beijing 100124, China;
2. Beijing Key Laboratory of Nonlinear Vibrations and Strength of Mechanical Structures, Beijing 100124, China;
3. School of Mechanical Engineering, Tianjin University of Technology, Tianjin 300384, China

(Received Apr. 16, 2019 / Revised Jun. 10, 2019)

Abstract Vibration energy harvesting is to transform the ambient mechanical energy to electricity. How to reduce the resonance frequency and improve the conversion efficiency is very important. In this paper, a layer-separated piezoelectric cantilever beam is proposed for the vibration energy harvester (VEH) for low-frequency and wide-bandwidth operation, which can transform the mechanical impact energy to electric energy. First, the electromechanical coupling equation is obtained by the Euler-Bernoulli beam theory. Based on the average method, the approximate analytical solution is derived and the voltage response is obtained. Furthermore, the physical prototype is fabricated, and the vibration experiment is conducted to validate the theoretical principle. The experimental results show that the maximum power of 0.445 μW of the layer-separated VEH is about 3.11 times higher than that of the non-impact harvester when the excitation acceleration is $0.2\,g$. The operating frequency bandwidth can be widened by increasing the stiffness of the fundamental layer and decreasing the gap distance of the system. But the increasing of operating frequency bandwidth comes at the cost of reducing peak voltage. The theoretical simulation and the experimental results demonstrate good agreement which indicates that the proposed impact-driving VEH device has advantages for low-frequency and wide-bandwidth. The high performance provides great prospect to scavenge the vibration energy in environment.

Key words vibration energy harvester (VEH), layer-separated piezoelectric beam, low-frequency, broad-bandwidth

Chinese Library Classification O242
2010 Mathematics Subject Classification 74S05

* Citation: CAO, D. X., XIA, W., and HU, W. H. Low-frequency and broadband vibration energy harvester driven by mechanical impact based on layer-separated piezoelectric beam. *Applied Mathematics and Mechanics* (*English Edition*), **40**(12), 1777–1790 (2019) https://doi.org/10.1007/s10483-019-2542-5

† Corresponding author, E-mail: caostar@bjut.edu.cn

Project supported by the National Natural Science Foundation of China (Nos. 11672008, 11702188, and 1832002)

1 Introduction

Energy harvesting technology refers to transform the ambient energy, such as solar, heat, sound, wind, and vibration, into electrical energy and store in capacitor or battery in a variety of ways. It is found that the harvesting efficiency of the vibration energy in the environment is as high as 25%–50%. Vibration energy harvesting is a promising technology as it could be used for low-power electronic components, which are widely applied in many engineering fields such as flexible electronics, wearable devices, and wireless sensor system. There are mainly three common electromechanical transformation mechanisms for vibration energy harvesting, i.e., the electromagnetic effect[1–2], the electrostatic effect[3–5], and the piezoelectric effect[6–10]. In recent years, the piezoelectric vibration energy harvesting (PVEH) attracts broad attention because of its advantages of high conversion efficiency and easy integration for microelectromechanical systems.

In nature and engineering fields, there is always lower-frequency environment vibration, while the oscillator frequency of the vibration energy harvester (VEH) is higher. It becomes significant to broaden the response bandwidth and improve the conversion efficiency for the VEH. To achieve this goal, scientists developed many kinds of oscillators based on linear and nonlinear vibration theory, such as bistable models[11–13], multistable models[14–16], and multi-degrees models[17–18]. There are also stochastic excitation VEHs[19–21] and nonlinear internal resonance VEHs[7,13,22].

In addition to the above-mentioned methods, many researchers proposed impact-driving VEH. Umeda et al.[23] earlier used a free-fall ball to collide a piezoelectric beam to harvest the low-frequency vibration energy. Halim et al.[24] and Halim and Park[25–26] designed several kinds of low-frequency VEHs using stopper-engaged dynamic magnifier. Liu et al.[27] proposed a stopper VEH to increase the energy conversion bandwidth by limiting the vibration amplitude through mechanical stoppers, while the power output was decreased. Li et al.[28] studied a bi-resonant PVEH to extend the operating frequency bandwidth. Yuan et al.[29] focused on the semi-analytical approach based on the harmonic balance method to predict steady-state responses of nonlinear piezoelectric vibration energy harvester, which consists of an oscillator of two magnetic beams. Dechant et al.[30] studied a new kind of low-frequency broadband VEH coupled with two mechanical stoppers, which significantly improves the vibration-to-electricity conversion efficiency by 40%–81%. Two-degree-of-freedom piecewise-linear PVEH was also studied by Liu et al.[31] and Zhao et al.[32], which demonstrates good harvesting performance.

In this paper, a new impact-driving PVEH is proposed for low-frequency and broadband vibration energy harvesting based on a layer-separated piezoelectric beam. Firstly, the generating mechanism of the impact-driving PVEH is introduced in Section 2, where the theoretical model is also constructed. The amplitude-frequency response and the numerical simulation are obtained in Section 3. The vibration experiment is then conducted for the impact-driving VEH and the effects of different parameters on the operating frequency bandwidth and output power of the system are discussed in Section 4. Finally, the conclusion is given.

2 Mechanical configuration and theoretical modeling

2.1 Mechanical configuration and working principle

As shown in Fig. 1, the proposed impact-driving PVEH is made up of a piezoelectric laminated cantilever beam and a tip mass at the free end, where the laminated beam includes a protective layer, a piezoelectric layer, and a fundamental layer. Here, the particularity of this structure is embodied in the separated layers between the piezoelectric layer and the fundamental layer. The piezoelectric layer is made of polyvinylidene fluoride (PVDF) sheet and used for energy conversion while the fundamental layer and the protective layer are made of the brass sheet and the polyester sheet, respectively. For the effect of the clamping force of the fixture,

a gap distance is formed between the fundamental layer and the piezoelectric layer.

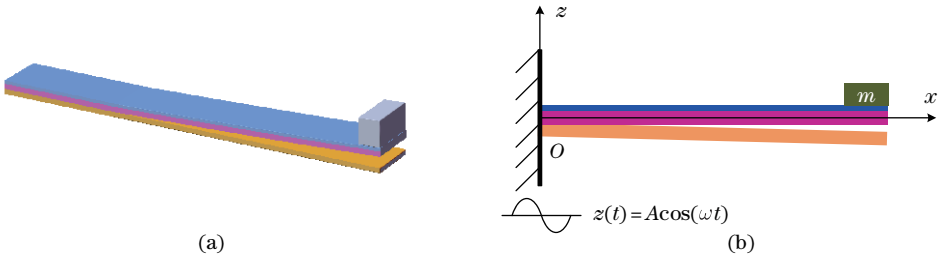

Fig. 1 The mechanical configuration of the proposed impact-driving PVEH, (a) the 3-dimensional schematic, and (b) the mechanical model with coordinate frame (color online)

When an external vibration with an appropriately large amplitude is imposed on the harvester, the separate piezoelectric layer with the protective layer begins to vibrate and the tip mass moves down over the gap distance producing an impact periodically onto the separate fundamental layer. During the impact, the separate fundamental layer acts as a stopper for its greater stiffness and the separate piezoelectric layer vibrates together with the separate fundamental layer for a short moment, leading to the increase of the stiffness of the separate piezoelectric layer which extends the resonance over a wider range. At the same time, for a smaller stiffness of the piezoelectric layer and the protective layer, the harvester can achieve lower vibration frequency and produce higher output voltage.

2.2 Theoretical modeling

In order to investigate the effects and potential benefits of the proposed impact-driving PVEH, the governing equation needs to be established and analyzed. But as the premise, it is necessary to introduce the following assumptions: (a) suppose the separate piezoelectric layer with the protective layer for a cantilever beam, and that the impact between the separate parts occurs only at the free ends of the piezoelectric layer and the fundamental layer, (b) suppose that the section plane of the beam is still perpendicular to the middle plane after transverse bending, (c) neglect the moment of inertia, and (d) only the transverse electric field is considered.

Based on the electromechanical coupling, the following linear constitutive equations could be used to compute the potential energy of the piezoelectric material:

$$\begin{cases} T_x = C_{xx}^E S_x - d_{zx} E_z, \\ D_z = d_{zx} S_x + \varepsilon_{zz}^{\mathrm{S}} E_z, \end{cases} \tag{1}$$

where T_x and S_x are the stress and the strain along the length of the beam, respectively. D_z is the electric displacement, while E_z is the electric field that develops through the thickness of the piezoelectric layer. C_{xx}^E is the Young's modulus of the piezoelectric layer. d_{zx} denotes the piezoelectric strain coefficient. $\varepsilon_{zz}^{\mathrm{S}}$ is the laminate permittivity.

The relationship between the nonlinear strain and transversal displacement is given as follows:

$$S_x = -z\left(v'' + \frac{1}{2}v'^2 v''\right), \tag{2}$$

where v is the transversal displacement. The notation $(')$ indicates the derivative with respect to x.

The kinetic energy of the system is expressed as follows:

$$T = \frac{1}{2}\int_0^L (\rho_{\mathrm{p}} b h_{\mathrm{p}} + \rho_{\mathrm{s}} b h_{\mathrm{s}})(\dot{v}(x,t) + \dot{z}(t))^2 \mathrm{d}x + \frac{1}{2} m (\dot{v}(L,t) + \dot{z}(t))^2, \tag{3}$$

where $\rho_{\rm p}$ and $\rho_{\rm s}$ are the densities of the piezoelectric layer and the protective layer, respectively. The notation $\dot{(\cdot)}$ indicates a time derivative while m is the tip mass and $z(t) = A\cos(\omega t)$ is the base motion. L is the effective length of the piezoelectric beam, and b is the width of the piezoelectric beam. $h_{\rm p}$ and $h_{\rm s}$ are the thicknesses of the piezoelectric layer and the protective layer, respectively.

The potential energy distributed along the length of the beam is given as follows:

$$U = \frac{1}{2}\int_{V_{\rm p}} (T_x S_x - D_z E_z)\mathrm{d}V_{\rm p} + \frac{1}{2}\int_{V_{\rm s}} E_{\rm s} S_x^2 \mathrm{d}V_{\rm s}, \tag{4}$$

where $E_{\rm s}$ is the Young's modulus of the protective layer. $V_{\rm p}$ and $V_{\rm s}$ are the volumes of the piezoelectric layer and the protective layer, respectively. The electric field E_z is expressed as follows by regarding the electrodes on the lower and upper surfaces of the piezoelectric layer as a single electrode pair:

$$E_z = -\frac{V}{h_{\rm p}}, \tag{5}$$

where V indicates the voltage of the system.

To obtain the ordinary differential equations, Galerkin's method with a trial function is used,

$$v(x,t) = \sum_{n=1}^{m} \phi_n(x)\, r_n(t), \tag{6}$$

where n indicates the mode shape number. To simplify the derivations, the first mode shape of the cantilever beam is used ($n = 1$),

$$\phi_1(x) = C_4\Big(\cosh(\lambda_1 x) - \cos(\lambda_1 x) - \frac{\cosh(\lambda_1 L) + \cos(\lambda_1 L)}{\sinh(\lambda_1 L) + \sin(\lambda_1 L)}(\sinh(\lambda_1 x) - \sinh(\lambda_1 x))\Big), \tag{7}$$

where C_4 is determined by the following equation:

$$(\rho_{\rm p} b h_{\rm p} + \rho_{\rm s} b h_{\rm s}) \int_0^L \varphi_1^2(x)\mathrm{d}x + m\varphi_1^2(L) = 1. \tag{8}$$

The frequency λ_1 can be expressed by

$$\lambda_1^2 = \omega_1 \sqrt{\frac{\rho_{\rm p} b h_{\rm p} + \rho_{\rm s} b h_{\rm s}}{C_{xx}^E I_{\rm p} + E_{\rm s} I_{\rm s}}}. \tag{9}$$

$I_{\rm p}$ and $I_{\rm s}$ are the moments of inertia of the fundamental layer and the piezoelectric layer, respectively, and can be described as follows:

$$I_{\rm p} = \frac{1}{3} b h_{\rm p}(3h_{\rm p}^2 - 3h_{\rm p}h_{\rm n} + h_{\rm n}^3), \quad I_{\rm s} = \frac{1}{3} b h_{\rm s}(3h_{\rm n}^2 + 3h_{\rm p}h_{\rm n} + h_{\rm s}^3), \tag{10}$$

where $h_{\rm n}$ is the position of the neutral axis and can be written as $h_{\rm n} = (C_{xx}^E h_{\rm p}^2 - E_{\rm s} h_{\rm s}^2)/(2(C_{xx}^E h_{\rm p} + E_{\rm s} h_{\rm s}))$. The first natural frequency of the piezoelectric cantilever beam ω_1 is determined by the boundary conditions of the cantilever beam as follows:

$$\begin{cases} \varphi_1(x) = 0 \quad \text{at} \quad x = 0, \\ \dfrac{\mathrm{d}\varphi_1(x)}{\mathrm{d}x} = 0 \quad \text{at} \quad x = 0, \\ (C_{xx}^E I_{\rm p} + E_{\rm s} I_{\rm s}) \dfrac{\mathrm{d}^2\varphi_1(x)}{\mathrm{d}x^2} = 0 \quad \text{at} \quad x = L, \\ (C_{xx}^E I_{\rm p} + E_{\rm s} I_{\rm s}) \dfrac{\mathrm{d}^3\varphi_1(x)}{\mathrm{d}x^3} = -m\omega_1^2 \varphi_1(x) \quad \text{at} \quad x = L. \end{cases} \tag{11}$$

The motion equation and the voltage equation of the system can be obtained by employing Lagrange's equations for electromechanical systems,

$$\begin{cases} \dfrac{\mathrm{d}}{\mathrm{d}t}\Big(\dfrac{\partial T}{\partial \dot{r}_1}\Big) - \dfrac{\partial T}{\partial r_1} + \dfrac{\partial U}{\partial r_1} = F_1, \\ \dfrac{\mathrm{d}}{\mathrm{d}t}\Big(\dfrac{\partial T}{\partial \dot{V}}\Big) - \dfrac{\partial T}{\partial V} + \dfrac{\partial U}{\partial V} = Q, \end{cases} \tag{12}$$

where F_1 is a generalized force and can be expressed as follows:

$$F_1 = \begin{cases} -c_1\dot{r}_1, \quad r_1 \geqslant -d/\varphi_1(L), \\ -(c_1+c_2)\dot{r}_1 - k_2(\varphi_1(L)r_1 + d), \quad r_1 < -d/\varphi_1(L). \end{cases} \tag{13}$$

Q is the generalized charge and can be obtained by

$$V = R_L\dot{Q}, \tag{14}$$

where R_L is the load resistance. c_1 and c_2 are the dampings of the separate piezoelectric layer with the protective layer and the separate fundamental layer, respectively. d is the gap distance, while k_2 is the stiffness of the separate fundamental layer, and can be expressed as follows:

$$k_2 = \frac{3E_bI_b}{L^3}, \tag{15}$$

where E_b and $I_b = bh_b^3/12$ are the Young's modulus and the moment of inertia of the separate fundamental layer, respectively.

Substituting Eqs. (3), (4), (13), and (14) into Eq. (12) yields the ordinary differential equation of the beam

$$\begin{cases} \ddot{r}_1 + 2\zeta_1\omega_1\,\dot{r}_1 + \omega_1^2 r_1 + f(\dot{r}_1,\, r_1) - \theta_1 V - \theta_2 r_1^2 V + \kappa\ddot{z} + \kappa_1 r_1^3 + \kappa_2 r_1^5 = 0, \\ C_{\mathrm{p}}\dot{V} + \dfrac{V}{R_L} + \theta_1\dot{r}_1 + \theta_2 r_1^2\dot{r}_1 = 0, \end{cases} \tag{16}$$

where

$$f(\dot{r}_1,\, r_1) = \begin{cases} 0, \quad r_1 \geqslant -\delta, \\ 2\zeta_2\omega_2\dot{r}_1 + \varphi_L k_2(r_1+\delta), \quad r_1 < -\delta, \end{cases} \tag{17}$$

$$\begin{cases} \omega_2 = \sqrt{k_2/(\rho_b L b h_b)}, \quad \zeta_1 = \dfrac{c_1}{2\omega_1}, \quad \zeta_2 = \dfrac{c_2}{2\omega_2}, \quad \theta_1 = \dfrac{1}{2}bd_{zx}(2h_{\mathrm{n}} - h_{\mathrm{p}})\displaystyle\int_0^L \varphi_1''\mathrm{d}x, \\ \theta_2 = \dfrac{3}{4}bd_{zx}(2h_n - h_{\mathrm{p}})\displaystyle\int_0^L \varphi_1'^2\varphi_1''\mathrm{d}x, \quad \kappa = (\rho_{\mathrm{p}}A_{\mathrm{p}} + \rho_{\mathrm{s}}A_{\mathrm{s}})\displaystyle\int_0^L \varphi_1\mathrm{d}x + m\varphi_1(L), \\ \kappa_1 = 2(C_{xx}^E I_{\mathrm{p}} + E_{\mathrm{s}}I_{\mathrm{s}})\displaystyle\int_0^L \varphi_1'^2\varphi_1''^2\mathrm{d}x, \quad \kappa_2 = \dfrac{3}{4}(C_{xx}^E I_{\mathrm{p}} + E_{\mathrm{s}}I_{\mathrm{s}})\displaystyle\int_0^L \varphi_1'^4\varphi_1''^2\mathrm{d}x, \\ C_{\mathrm{p}} = \dfrac{Lb\varepsilon_{zz}^{\mathrm{S}}}{h_{\mathrm{p}}}, \quad \delta = d/\varphi_1(L), \quad \varphi_L = \varphi_1(L). \end{cases} \tag{18}$$

3 Theoretical analysis

3.1 Frequency response equation

When the ratio of deflection to length is less than 1/3 under the appropriate external excitation, the energy harvesting system can be considered as a piecewise-linear system. Therefore, the dynamic equation of the piecewise-linear system can be obtained by ignoring the second,

the third, and the fifth terms of the dynamic equation (16), and can be analyzed by the average method[26,32],

$$\begin{cases} \ddot{r}_1 + b_1 r_1 = F, \\ \dot{V} + b_2 \dot{r}_1 + b_3 V = 0, \end{cases} \tag{19}$$

where

$$F = -\kappa \ddot{z} - 2\zeta_1 \omega_1 \dot{r}_1 - f(\dot{r}_1, r_1) + \theta_1 V, \tag{20}$$

$$b_1 = \omega_1^2, \quad b_2 = \frac{\theta_1}{C_{\mathrm{p}}}, \quad b_3 = \frac{1}{C_{\mathrm{p}} R_L}. \tag{21}$$

The corresponding derived linear system of Eq. (19) is obtained by ignoring the parameter F, and its solution can be obtained as follows:

$$\begin{cases} r_1 = B\cos\psi, \\ \dot{r}_1 = -B\omega_1 \sin\psi, \\ V = -\dfrac{Bb_2\omega_1}{\omega_1^2 + b_3^2}(\omega_1 \cos\psi - b_3 \sin\psi), \end{cases} \tag{22}$$

where B and $\psi = \omega\, t + \theta$ represent the amplitude and the phase angle of the displacement r_1, respectively. θ represents the difference between the phase angles of the displacement and the excitation. For the nonlinear equation (19), B and θ are variables relative to time. Therefore, the nonlinear system can be analyzed by analyzing the amplitude and the phase difference of the displacement r_1.

According to the first and the second formulas of Eq. (22), we can get

$$\frac{\mathrm{d}B}{\mathrm{d}t}\cos\psi - B\frac{\mathrm{d}\theta}{\mathrm{d}t}\sin\psi = B(\omega - \omega_1)\sin\psi. \tag{23}$$

By substituting the linear solution of Eq. (22) into the first formula of the nonlinear equation (19), we can obtain

$$\frac{\mathrm{d}B}{\mathrm{d}t}\sin\psi + B\frac{\mathrm{d}\theta}{\mathrm{d}t}\cos\psi = -\frac{F}{\omega_1} - B(\omega - \omega_1)\cos\psi. \tag{24}$$

The parameter F is also replaced by the linear solution of Eq. (22), and can be expressed as

$$F = \kappa A\omega^2 \cos\omega t + 2B\zeta_1\omega_1^2 \sin\psi - f(B,\ \psi) - \frac{B\theta_1 b_2 \omega_1}{\omega_1^2 + b_3^2}(\omega_1 \cos\psi - b_3 \sin\psi), \tag{25}$$

where the nonlinear term is transformed with the first order Fourier transformation, and can be expressed as follows:

$$f(B,\ \psi) = \frac{2}{\pi}\varphi_L k_2 B(\psi_0 \cos\psi_0 - \sin\psi_0) + \frac{1}{\pi}Bh_0(\varphi_L k_2 \cos\psi - 2\omega_1\omega_2\zeta_2 \sin\psi), \tag{26}$$

where $\psi_0 = \arccos(\delta/B)$ indicates the displacement of the system corresponding to the phase angle of the whole periodic motion when the separate piezoelectric layer collides with the separate fundamental layer, and $h_0 = \psi_0 - \sin\psi_0 \cos\psi_0$.

The expressions of $\mathrm{d}B/\mathrm{d}t$ and $\mathrm{d}\theta/\mathrm{d}t$ can be obtained by Eqs. (23) and (24),

$$\begin{cases} \dfrac{\mathrm{d}B}{\mathrm{d}t} = -\dfrac{F}{\omega_1}\sin\psi, \\ \dfrac{\mathrm{d}\theta}{\mathrm{d}t} = -\dfrac{F}{\omega_1 B}\cos\psi + \omega_1 - \omega. \end{cases} \tag{27}$$

We assume that the average values of phase angle θ and amplitude B are constant in a complete period. So the expressions of $\mathrm{d}B/\mathrm{d}t$ and $\mathrm{d}\theta/\mathrm{d}t$ can be expressed by the average method,

$$\begin{cases} \dfrac{\mathrm{d}B}{\mathrm{d}t} = \dfrac{1}{2\pi}\displaystyle\int_0^{2\pi} \Big(-\frac{F}{\omega_1}\sin\psi\Big)\mathrm{d}\psi = \frac{\kappa A\omega^2}{2\omega_1}\sin\theta - \eta_{\mathrm{e}}(B)B, \\ \dfrac{\mathrm{d}\theta}{\mathrm{d}t} = \dfrac{1}{2\pi}\displaystyle\int_0^{2\pi} \Big(-\frac{F}{\omega_1 B}\cos\psi + \omega_1 - \omega\Big)\mathrm{d}\psi = -\frac{\kappa A\omega^2}{2B\omega_1}\cos\theta + \omega_{\mathrm{e}}(B) - \omega, \end{cases} \tag{28}$$

where parameters $\omega_{\mathrm{e}}(B)$ and $\eta_{\mathrm{e}}(B)$ represent the equivalent natural frequency and the attenuation coefficient of the amplitude function B, respectively,

$$\begin{cases} \omega_{\mathrm{e}}(B) = \omega_1 + \dfrac{\theta_1 b_2\omega_1}{2(\omega_1^2 + b_3^2)} + \dfrac{\varphi_L k_2 h_0}{2\pi\omega_1}, \\ \eta_{\mathrm{e}}(B) = \zeta_1\omega_1 + \dfrac{\theta_1 b_2 b_3}{2(\omega_1^2 + b_3^2)} + \dfrac{\omega_2\zeta_2 h_0}{\pi}. \end{cases} \tag{29}$$

As discussed above, the approximate values of $\mathrm{d}B/\mathrm{d}t$ and $\mathrm{d}\theta/\mathrm{d}t$ can be assumed to be zero. Therefore, Eq. (28) can be transformed as

$$\kappa A\omega^2\sin\theta = 2\omega_1\eta_{\mathrm{e}}(B)B, \tag{30}$$

$$\kappa A\omega^2\cos\theta = 2\omega_1(\omega_{\mathrm{e}}(B) - \omega)B. \tag{31}$$

Since the separate piezoelectric layer vibrates in the resonance region, the parameter $2\omega_1$ in Eq. (30) can be approximately replaced by 2ω. The parameter $2\omega_1$ in Eq. (31) can be approximately replaced by $\omega_{\mathrm{e}}(B) + \omega$. Then, the expression of the amplitude-frequency response of amplitude B relative to the excitation frequency can be obtained as follows:

$$B = \frac{\kappa A\omega^2}{\sqrt{(\omega_{\mathrm{e}}^2(B) - \omega^2)^2 + (2\omega\eta_{\mathrm{e}}(B))^2}}. \tag{32}$$

According to Eq. (22), the relationship between the voltage amplitude V and the displacement amplitude B can be obtained as follows:

$$V = \frac{b_2\omega_1}{\sqrt{\omega_1^2 + b_3^2}}B. \tag{33}$$

3.2 Analytical results

In this section, the parameters of the proposed energy harvester are set as Table 1. In order to get the open circuit voltage of the system, the load resistance R_L is set as 20 MΩ, which is far greater than its internal impedance. Substituting the parameters in Table 1 into Eq. (33), the open circuit voltage of the proposed energy harvester can be obtained. The results are shown by the red curve in Fig. 2, which illustrates the variation of the open circuit voltage with the external excitation frequency. At the same time, the open circuit voltage versus the external excitation frequency of the original harvester is shown by the blue curve. The entire red curve can be divided into three stages when the frequency increases from 0 Hz to 300 Hz. Stage I starts from Point A to Point B, where the open circuit voltage grows with the excitation frequency. Stage Ⅱ starts from Point B to Point C, where the end of the separate piezoelectric layer with the tip mass reaches the gap distance d and starts to impact the separate fundamental layer. During the impact (Stage Ⅱ), the stiffness and damping of the separate piezoelectric with the protective layer are increased due to that of the separate fundamental layer, and the amplitude-frequency response curve of output voltage presents a multi-solution phenomenon,

in which the red solid line shows the stable solution while the green dashed line represents the unstable solution. As a result, the equivalent resonance frequency is enlarged. Therefore, the operating frequency bandwidth of the harvester is broadened. Stage III starts when the excitation frequency reaches Point C, where the hard spring characteristic happens and the open circuit voltage of the system drops dramatically to Point D. Then, the open circuit voltage decreases gradually when the excitation frequency changes from Point D to Point E.

Table 1 The parameters of the proposed energy harvester

Position	Parameter	Value
Beam	Length L	25 mm
	Width b	10 mm
	Tip mass m	0.001 5 kg
	Damping c_1	0.439 kg·s^{-1}
Piezoelectric layer	Young's modulus C_{xx}^E	2.5 GPa
	Piezoelectric strain coefficient d_{zx}	–18 pC/N
	Thickness h_{p}	0.3 mm
	Laminate permittivity $\varepsilon_{zz}^{\mathrm{S}}$	2.18 nF/m
	Capacitance of piezoelectric layer C_{p}	1.82 nF
	Density ρ_{p}	2 000 kg/m^3
Protective layer	Young's modulus E_{s}	3 GPa
	Thickness h_{s}	0.1 mm
	Density ρ_{s}	1 000 kg/m^3
Fundamental layer	Young's modulus E_b	90 GPa
	Density ρ_b	8 900 kg/m^3
	Damping c_2	3.328 kg·s^{-1}

As demonstrated by the blue curve, the open circuit voltage grows with the increase of the excitation frequency, and then decreases gradually. From the comparison of the two curves, we can see that the resonance frequency of the separate energy harvester is much smaller than that of the original energy harvester. It is well known that under the same external excitation acceleration, a system will have large amplitude when the external excitation frequency is small. Therefore, the separate energy harvester can harvest low-frequency vibration energy and output larger voltage. At the same time, since the separate parts collide with each other during the vibration process, the operating frequency bandwidth of the system can be widened. Obviously, the separate energy harvester, as a miniature device, has great advantages in collecting low-frequency vibration energy.

The gap distance d and the stiffness of the separate fundamental layer k_2 are two important parameters for the power generation of the system. According to Eq. (15), the value of k_2 depends on the thickness of the fundamental layer h_b, and the values of k_2 are 388.8 N/m, 921.6 N/m, 1 800.0 N/m, and 3 100.4 N/m when the values of h_b are 0.3 mm, 0.4 mm, 0.5 mm, and 0.6 mm, respectively. In order to find out the effect of the change of k_2 on the output voltage, the external excitation acceleration $a = A\omega^2$ is set to $0.2\,g$, and the gap distance d is set to 0.5 mm. Figure 3 depicts the curve of open circuit voltage versus the frequency when k_2 takes different values (388.8 N/m, 921.6 N/m, 1 800.0 N/m, and 3 100.4 N/m). As shown in the figure, with the increase value of k_2, the peak voltage of the system will decrease while the operating frequency bandwidth becomes wider. The reason is that a greater k_2 will increase the values of the equivalent stiffness and the equivalent damping when the separate parts collide with each other. Therefore, as discussed above, the values of the operating frequency bandwidth will be broadened. The operating frequency bandwidth are 3.6 Hz, 5.8 Hz, and 8.9 Hz when the values of k_2 are 388.8 N/m, 921.6 N/m, and 1 800.0 N/m, respectively. Meanwhile, the greater equivalent damping reduces the amplitude of the separate piezoelectric layer, resulting in a reduction of the open circuit voltage.

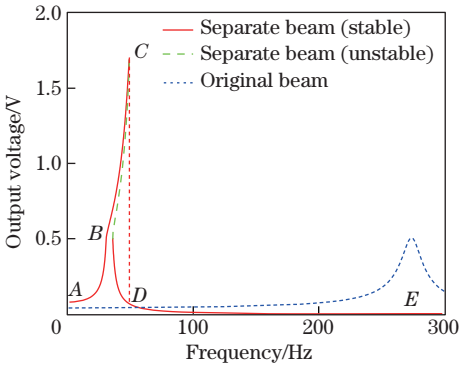

Fig. 2 The analytical results for the open circuit voltage of the impact-driving PVEH and the original non-impact PVEH (color online)

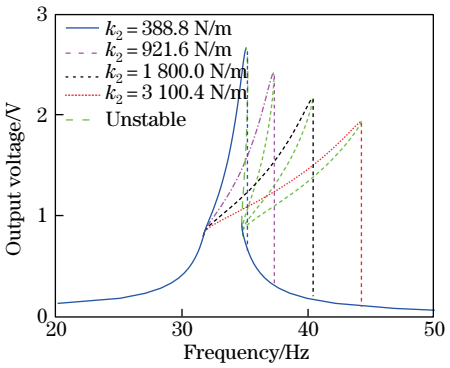

Fig. 3 The analytical results for the open circuit voltage with different impact stiffness k_2 (color online)

In order to find out the influence of the parameter d on the generation law of the system, the external excitation acceleration a is set to $0.2\,g$, and the impact stiffness k_2 is set to $1\,800.0\,\mathrm{N/m}$. Figure 4 shows the curve of the open circuit voltage versus the frequency when d takes different values (0.2 mm, 0.5 mm, 0.8 mm, 1.0 mm, and 1.5 mm). As it can be seen from the figure, the operating frequency bandwidth is widened while the peak voltage is reduced with the gap distance decreases. The separate piezoelectric layer impacts the fundamental layer early when d is small, bringing in an increase of the stiffness and the damping at an early time. Meanwhile, a small gap distance can enlarge the impact frequency range. Thus, the peak voltage will be decreased and the operating frequency bandwidth will be broadened.

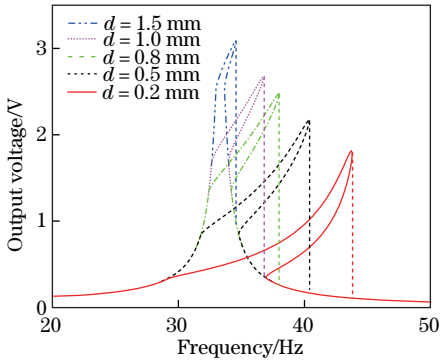

Fig. 4 The analytical results for the open circuit voltage with different gap distance d (color online)

4 Experimental research

4.1 Experimental setup

The fabricated prototype is shown in Fig. 5. The protective layer and the fundamental layer are bonded on the two surfaces of the polarized piezoelectric layer. The effective length and the width of the beam are 25 mm and 10 mm, respectively. The thickness of the piezoelectric layer and the protective layer are 0.3 mm and 0.1 mm, respectively. The piezoelectric beams with the piezoelectric layers of 0.3 mm, 0.4 mm, and 0.5 mm are used in the experiment. A tip mass is fixed on the upper surface of the end of the beam. In the experiment, the piezoelectric layer is separated from the fundamental layer according to the need, and ensured that the gap at the

end of the separate parts to be 0.5 mm by the clamping force from the fixture. The fixture is fixed on the vibration exciter.

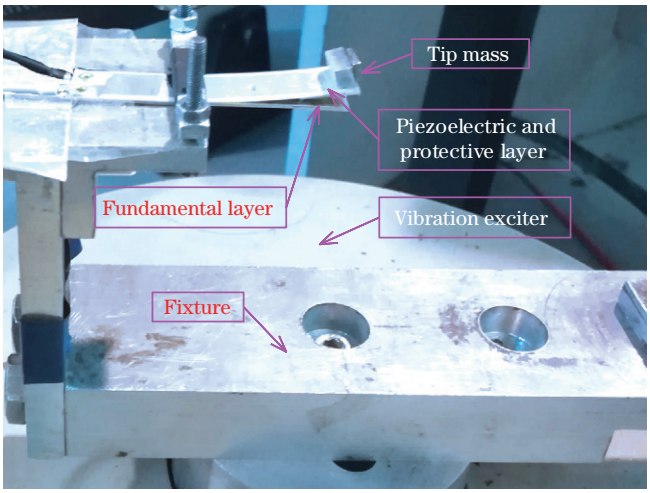

Fig. 5 The fabricated prototype of the proposed impact-driving PVEH (color online)

The experimental set-ups are shown in Fig. 6. It includes a signal generator, a power amplifier, an electric vibration exciter, a laser displacement sensor, a signal acquisition, a digital oscilloscope, multimeter, and a signal analysis software. Figure 7 shows the flow chart of signal in the experimental process. The signals are sent to the power amplifier by the signal generator. The power amplifier conveys the processed signal to the vibration exciter to control vibration of the piezoelectric energy harvester. Keeping the external excitation acceleration as $0.2\,g$, the excitation frequency is gradually increased from 0 Hz to 300 Hz by adjusting the signal generator. The output voltage is recorded by a digital oscilloscope directly. The deflection of piezoelectric beam under different excitation accelerations is measured by the laser displacement sensor to ensure that the movement of the beam is not a large deformation movement.

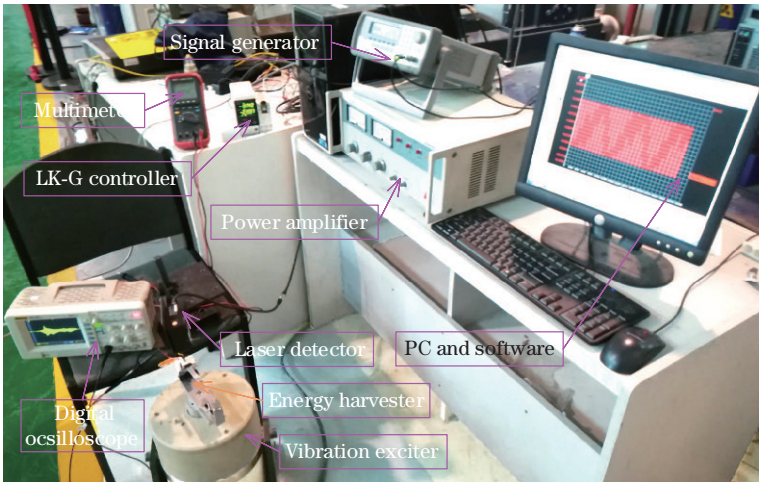

Fig. 6 The experimental set-ups (color online)

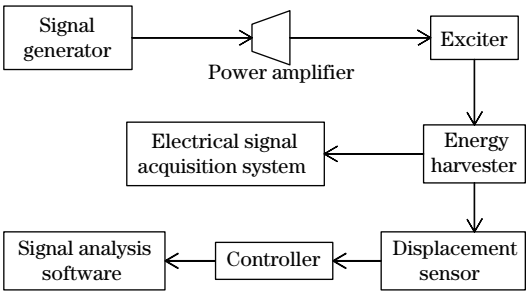

Fig. 7 The flow chart of signal processing

4.2 Experimental results

Figure 8 shows the comparison of the open circuit voltage of experimental results with theoretical results. Here, the red dotted curve shows the theoretical result and the blue triangular curve is the experimental result of the proposed harvester with $k_2 = 388.8\,\mathrm{N/m}$ and $d = 0.5\,\mathrm{mm}$ while the pink solid curve shows the theoretical result and the black dot curve is the experimental result of the original harvester. As can be seen from the figure, the peak voltage of the proposed harvester is higher than that of the original harvester, and the excitation frequency at peak voltage of the proposed harvester is much less than that of the original harvester. That is to say, the proposed harvester is more beneficial to harvest low-frequency vibration energy and acquire high output voltage. The operating frequency bandwidth in the experimental curve is 7.9 Hz more than the theoretical one, while the peak open circuit voltage is 2.12 V less than the theoretical one. The relative errors are calculated as 54.4% and 19.7%, respectively. Those errors are mostly caused by modeling, installation, and measurement. Although some errors occurred in the experimental results, the waveform curve of the open circuit voltage and the performance of broadening the operating frequency bandwidth and improving the peak voltage agreed well with the theoretical results. Therefore, the theoretical model and the analytical solution are proved suitable and can be further optimized.

Figure 9 shows the experimental open circuit voltage for different k_2 when $d = 0.5\,\mathrm{mm}$. The red curve and the blue curve show the open circuit voltage of the proposed harvester when the values of k_2 are 921.6 N/m and 1 800.0 N/m, respectively. The operating frequency bandwidth in the experimental curve is 8.6 Hz more than the theoretical one while the peak open circuit voltage is 1.94 V less than the theoretical one, when the value of k_2 is 921.6 N/m. The relative errors are calculated as 17.2% and 19.5%, respectively. The operating frequency bandwidth in the experimental curve is 10.7 Hz more than the theoretical one while the peak open circuit voltage is 1.71 V less than the theoretical one when the value of k_2 is 1 800.0 N/m. The relative errors are calculated as 16.8% and 20.4%, respectively. From the analysis above, we know that the operating frequency bandwidth increases gradually with the increase of the value of k_2 while the relative error of the operating frequency bandwidth of the experimental and theoretical results decrease gradually.

In order to measure the load voltage and the output power of the system, an adjustable load resistance with the variation ranging from 0 MΩ to 12 MΩ which can cover the optimum value is connected to two electrodes of the harvester, and the load voltage is measured by adjusting the value of the resistance. The load voltages and the output powers of the original harvester and the separate harvester with $k_2 = 388.8\,\mathrm{N/m}$ and $d = 0.5\,\mathrm{mm}$ versus the resistance are shown in Fig. 10. As can be seen from the figure, the maximum output power 0.445 μW of the separate harvester is obtained when the load resistance is 2.5 MΩ at 36 Hz while the maximum power 0.143 μW of the original harvester is obtained when the load resistance is 0.34 MΩ at 265 Hz. The maximum load voltage and the maximum power of the separate harvester are about 4.78 and 3.11 times higher than those of the original harvester, respectively. The impedance of

piezoelectric layer can be calculated by $R_s = 1/(2\pi f C_p)$. When the impedance of piezoelectric layer R_s equals the load resistance R_L, the output power reaches the maximum.

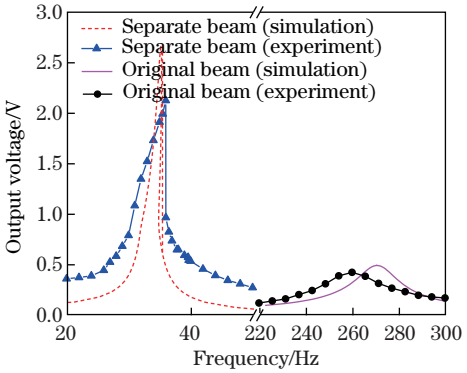

Fig. 8 The comparison of the open circuit voltage of experimental results with theoretical results (color online)

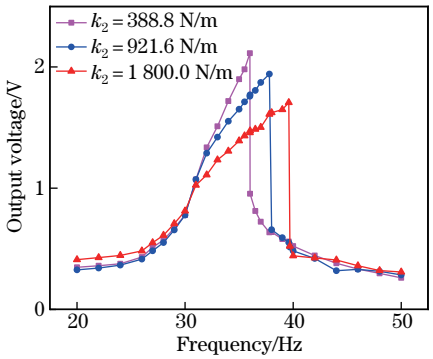

Fig. 9 The experimental results for the open circuit voltage with different k_2 (color online)

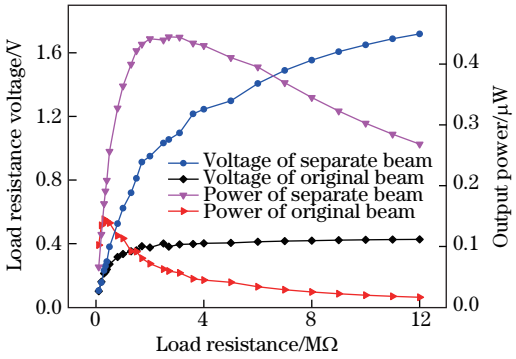

Fig. 10 The load resistance voltage and the output power of the impact-driving PVEH and the non-impact PVEH (color online)

5 Conclusions

In this paper, an impact-driving piezoelectric vibration energy harvester is proposed for a lower resonance frequency and a higher output power based on a layer-separated piezoelectric laminated cantilever beam. The working mechanism and the theoretical model are introduced in detail. When the ratio of the deflection to length is less than 1/3 under the appropriate external excitation, the separate piezoelectric harvester can be considered as a piecewise-linear system by ignoring higher order nonlinear terms of the governing equation. The approximate analytical solution is obtained based on the average method. The numerical simulation and vibration test are also conducted and all the results demonstrate the advantages of the vibration energy harvesting for the lower resonance frequency and the higher output power. The operating frequency bandwidth can be widened by increasing the stiffness of the fundamental layer and decreasing the gap distance of the system. But the increasing of operating frequency bandwidth comes at the cost of reducing peak voltage. The maximum power of 0.445 μW of the separate harvester is about 3.11 times higher than that of the original harvester when the

excitation acceleration is $0.2\,g$. Although there are little quantitive errors between the analytical and experimental results, the qualitative results are well consistent with each other. In view of the close agreement of the variation trend between the theoretical values and experimental results, the proposed impact-driving PVEH could be applied to further micro-electromechanical system (MEMS) fabrication process and optimized design.

References

[1] FANG, Z. W., ZHANG, Y. W., LI, X., DING, H., and CHEN, L. Q. Integration of a nonlinear energy sink and a giant magnetostrictive energy harvester. *Journal of Sound and Vibration*, **391**, 35–49 (2017)

[2] ZOU, H., ZHANG, W., LI, W., WEI, K., HU, K., PENG, Z., and MENG, G. Magnetically coupled flextensional transducer for wideband vibration energy harvesting: design, modeling and experiments. *Journal of Sound and Vibration*, **416**, 55–79 (2018)

[3] PEREZ, M., BOISSEAU, S., GASNIER, P., WILLEMIN, J., GEISLER, M., and REBOUD, J. L. A cm scale electret-based electrostatic wind turbine for low-speed energy harvesting applications. *Smart Materials and Structures*, **25**(4), 045015 (2016)

[4] ZHANG, X., PONDROM, P., SESSLER, G. M., and MA, X. Ferroelectret nanogenerator with large transverse piezoelectric activity. *Nano Energy*, **50**, 52–61 (2018)

[5] ANTON, S. R., FARINHOLT, K. M., and ERTURK, A. Piezoelectret foam-based vibration energy harvesting. *Journal of Intelligent Material Systems and Structures*, **25**(14), 1681–1692 (2014)

[6] LU, Z. Q., LI, K., DING, H., and CHEN, L. Q. Nonlinear energy harvesting based on a modified snap-through mechanism. *Applied Mathematics and Mechanics* (*English Edition*), **40**(1), 167–180 (2019) https://doi.org/10.1007/s10483-019-2408-9

[7] CAO, D. X., LEADENHAM, S., and ERTURK, A. Internal resonance for nonlinear vibration energy harvesting. *European Physical Journal-Special Topics*, **224**(14-15), 2867–2880 (2015)

[8] CAO, D. X., GUO, X. Y., and HU, W. H. A novel low-frequency broadband piezoelectric energy harvester combined with a negative stiffness vibration isolator. *Journal of Intelligent Material Systems and Structures*, **30**(7), 1105–1114 (2019)

[9] ZHANG, W., YAO, Z., and YAO, M. Periodic and chaotic dynamics of composite laminated piezoelectric rectangular plate with one-to-two internal resonance. *Science China-Technological Sciences*, **52**(3), 731–742 (2009)

[10] ZHANG, W., WU, Q. L., and MA, W. S. Chaotic wave motions and chaotic dynamic responses of piezoelectric laminated composite rectangular thin plate under combined transverse and in-plane excitations. *International Journal of Applied Mechanics*, **10**(10), 28 (2018)

[11] ERTURK, A., HOFFMANN, J., and INMAN, D. J. A piezomagnetoelastic structure for broadband vibration energy harvesting. *Applied Physics Letters*, **94**(25), 254102 (2009)

[12] SUN, S. and CAO, S. Q. Analysis of chaos behaviors of a bistable piezoelectric cantilever power generation system by the second-order Melnikov function. *Acta Mechanica Sinica*, **33**(1), 200–207 (2017)

[13] LAN, C., QIN, W., and DENG, W. Energy harvesting by dynamic unstability and internal resonance for piezoelectric beam. *Applied Physics Letters*, **107**(9), 093902 (2015)

[14] ZHOU, S., CAO, J., INMAN, D. J., LIN, J., LIU, S., and WANG, Z. Broadband tristable energy harvester: modeling and experiment verification. *Applied Energy*, **133**, 33–39 (2014)

[15] ZHOU, S. and ZUO, L. Nonlinear dynamic analysis of asymmetric tristable energy harvesters for enhanced energy harvesting. *Communications in Nonlinear Science and Numerical Simulation*, **61**, 271–284 (2018)

[16] LAI, S. K., WANG, C., and ZHANG, L. H. A nonlinear multi-stable piezomagnetoelastic harvester array for low-intensity, low-frequency, and broadband vibrations. *Mechanical Systems and Signal Processing*, **122**, 87–102 (2019)

[17] YUAN, T. C., YANG, J., and CHEN, L. Q. Nonlinear dynamics of a circular piezoelectric plate for vibratory energy harvesting. *Communications in Nonlinear Science and Numerical Simulation*, **59**, 651–656 (2018)

[18] ZHAO, L. C., ZOU, H. X., YAN, G., ZHANG, W. M., PENG, Z. K., and MENG, G. Arbitrary-directional broadband vibration energy harvesting using magnetically coupled flextensional transducers. *Smart Materials and Structures*, **27**(9), 095010 (2018)

[19] LIU, D., XU, Y., and LI, J. L. Probabilistic response analysis of nonlinear vibration energy harvesting system driven by Gaussian colored noise. *Chaos Solitons & Fractals*, **104**, 806–812 (2017)

[20] LU, Z. Q., CHEN, L. Q., BRENNAN, M. J., YANG, T., DING, H., and LIU, Z. G. Stochastic resonance in a nonlinear mechanical vibration isolation system. *Journal of Sound and Vibration*, **370**, 221–229 (2016)

[21] LIU, D., XU, Y., and LI, J. Randomly-disordered-periodic-induced chaos in a piezoelectric vibration energy harvester system with fractional-order physical properties. *Journal of Sound and Vibration*, **399**, 182–196 (2017)

[22] LU, Z. Q., DING, H., and CHEN, L. Q. Resonance response interaction without internal resonance in vibratory energy harvesting. *Mechanical Systems and Signal Processing*, **121**, 767–776 (2019)

[23] UMEDA, M., NAKAMURA, K., and UEHA, S. Analysis of the transformation of mechanical impact energy to electric energy using piezoelectric vibrator. *Japanese Journal of Applied Physics Part* 1-*Regular Papers Short Notes & Review Papers*, **35**(5B), 3267–3273 (1996)

[24] HALIM, M. A., KIM, D. H., and PARK, J. Y. Low frequency vibration energy harvester using stopper-engaged dynamic magnifier for increased power and wide bandwidth. *Journal of Electrical Engineering & Technology*, **11**(3), 707–714 (2016)

[25] HALIM, M. A. and PARK, J. Y. Piezoceramic based wideband energy harvester using impact-enhanced dynamic magnifier for low frequency vibration. *Ceramics International*, **41**, S702–S707 (2015)

[26] HALIM, M. A. and PARK, J. Y. Theoretical modeling and analysis of mechanical impact driven and frequency up-converted piezoelectric energy harvester for low-frequency and wide-bandwidth operation. *Sensors and Actuators A*: *Physical*, **208**, 56–65 (2014)

[27] LIU, H., LEE, C., KOBAYASHI, T., TAY, C. J., and QUAN, C. Investigation of an MEMS piezoelectric energy harvester system with a frequency-widened-bandwidth mechanism introduced by mechanical stoppers. *Smart Materials and Structures*, **21**(3), 035005 (2012)

[28] LI, S., CROVETTO, A., PENG, Z., ZHANG, A., HANSEN, O., WANG, M., LI, X., and WANG, F. Bi-resonant structure with piezoelectric PVDF films for energy harvesting from random vibration sources at low frequency. *Sensors and Actuators A*: *Physical*, **247**, 547–554 (2016)

[29] YUAN, T. C., YANG, J., and CHEN, L. Q. A harmonic balance approach with alternating frequency/time domain progress for piezoelectric mechanical systems. *Mechanical Systems and Signal Processing*, **120**, 274–289 (2019)

[30] DECHANT, E., FEDULOV, F., CHASHIN, D. V., FETISOV, L. Y., FETISOV, Y. K., and SHAMONIN M. Low-frequency, broadband vibration energy harvester using coupled oscillators and frequency up-conversion by mechanical stoppers. *Smart Materials and Structures*, **26**(6), 065021 (2017)

[31] LIU, S., CHENG, Q., ZHAO, D., and FENG, L. Theoretical modeling and analysis of two-degree-of-freedom piezoelectric energy harvester with stopper. *Sensors and Actuators A*: *Physical*, **245**, 97–105 (2016)

[32] ZHAO, D., LIU, S., XU, Q., SUN, W., WANG, T., and CHENG, Q. Theoretical modeling and analysis of a 2-degree-of-freedom hybrid piezoelectric-electromagnetic vibration energy harvester with a driven beam. *Journal of Intelligent Material Systems and Structures*, **29**(11), 2465–2476 (2018)